The American Journal of Pathology, Vol. 184, No. 3, March 2014

ELSEVIER

The American Journal of PATHOLOGY

ajp.amjpathol.org

NEUROBIOLOGY

Giant Axon Formation in Mice Lacking Kell, XK, or Kell and XK

Animal Models of McLeod Neuroacanthocytosis Syndrome

Xiang Zhu,*† Eun-Sook Cho,‡ Quan Sha,†§ Jianbin Peng,† Yelena Oksov,† Siok Yuen Kam,¶ Mengfatt Ho,¶ Ruth H. Walker,‖** and Soohee Lee†

From the Department of Pathology, Peking University Health Science Center, Beijing, China; the New York Blood Center,† New York, New York; the Department of Pathology and Laboratory Medicine (Neuropathology),‡ Rutgers University—New Jersey Medical School, Newark, New Jersey; the Department of Cell Line Development,§ Immunomedics, Morris Plains, New Jersey; the Division of Medical Sciences,¶ National Cancer Center, Singapore; the Department of Neurology,‖ James J. Peters VAMC, Bronx, New York; and the Department of Neurology,** Mount Sinai School of Medicine, New York, New York*

Accepted for publication November 13, 2013.

Address correspondence to Xiang Zhu, M.D., Ph.D., Peking University Health Science Center, Department of Pathology, Beijing 100191, China. E-mail: zhuxiangbjmu@163.com or zhuxiang@bjmu.edu.cn.

McLeod neuroacanthocytosis syndrome (MLS) is a rare X-linked multisystem disease caused by *XK* gene mutations and characterized by hematological and neurological abnormalities. XK, a putative membrane transporter, is expressed ubiquitously and is covalently linked to Kell, an endothelin-3-converting enzyme (ECE-3). Absence of XK results in reduction of Kell at sites where both proteins are coexpressed. To elucidate the functional roles of XK, Kell, and the XK—Kell complex associated with pathogenesis in MLS, we studied the pathology of the spinal cord, anterior roots, sciatic nerve, and skeletal muscle from knockout mouse models, using $Kel^{-/-}$, $Xk^{-/-}$, $Kel^{-/-}Xk^{-/-}$, and wild-type mice aged 6 to 18 months. A striking finding was that giant axons were frequently associated with paranodal demyelination. The pathology suggests probable anterograde progression from the spinal cord to the sciatic nerve. The neuropathological abnormalities were found in all three genotypes, but were more marked in the double-knockout $Kel^{-/-}Xk^{-/-}$ mice than in either $Kel^{-/-}$ or $Xk^{-/-}$ mice. Skeletal muscles from $Xk^{-/-}$ and $Kel^{-/-}Xk^{-/-}$ mice showed mild abnormalities, but those from $Kel^{-/-}$ mice were similar to the wild type. The more marked neuropathological abnormalities in $Kel^{-/-}Xk^{-/-}$ mice suggest a possible functional association between XK and Kell in nonerythroid tissues. *(Am J Pathol 2014, 184: 800—807; http://dx.doi.org/10.1016/j.ajpath.2013.11.013)*

McLeod neuroacanthocytosis syndrome (MLS) is a rare, X-linked multisystem disorder associated with the McLeod phenotype due to mutations in the *XK* gene. MLS typically presents in middle age, with central nervous system, neuromuscular, cardiac, and hematological manifestations. Abnormalities include acanthocytosis, cardiomyopathy, degeneration of the basal ganglia, and sensorimotor neuropathy. Central nervous system manifestations include chorea and cognitive and psychiatric abnormalities similar to those seen in Huntington disease.[1–3] Acanthocytosis accompanied by compensated hemolysis and a variable reaction to incompatible transfusion may occur because of the McLeod blood-group phenotype. Neurodegeneration affects mainly the caudate nucleus, although functional neuroimaging demonstrates more general striatal pathology, with decreased dopamine D_2 receptor binding, decreased [^{18}F]fluorodeoxyglucose uptake, and caudate hypoperfusion. Neuromuscular manifestations include sensorimotor axonopathy, as well as myopathy with elevated creatine kinase. Histopathological studies indicate axonal degeneration of the sural nerve and neurogenic atrophy in most muscle studies, with fiber atrophy in some cases. Additional nonspecific changes include internalized nuclei and variation in muscle fiber sizes.[4]

The putative membrane transporter XK, a member of the XK family, is expressed ubiquitously. It is linked to the endothelin-3-converting enzyme Kell via a single disulfide bond when they are coexpressed (eg, in red blood cells). Insights into XK—Kell function can be gained from XK binding to the 4.1R protein. Linked to Kell, XK binds to the α-lobe (B lobe, middle lobe) of the FERM domain of protein 4.1R,

Supported by NIH grant R01 HL075716 (S.L.).
Disclosures: None declared.

http://dx.doi.org/10.1016/j.ajpath.2013.11.013

which itself binds to β-spectrin at the binding junction of spectrin and actin, forming a 4.1R–spectrin–actin ternary complex of cytoskeleton in erythrocytes.[5–8]

Although Kell and XK are covalently linked on red blood cells, where each protein appears to be expressed in equal amounts, XK is expressed in relatively large amounts in nonerythroid tissues, such as skeletal muscle and brain.[9–12] In contrast, Kell is largely restricted to erythroid tissues, although a small amount is expressed in nonerythroid tissues such as spinal cord and probably in specific functional cells in brain.[11,13,14] The expression of Kell and XK in red blood cell membranes is closely linked; when Kell is absent, XK is reduced, and vice versa. In human skeletal muscle, XK is expressed in type 2 fibers.[15]

To study the physiological functions of Kell and XK, and their interactions, $Kel^{-/-}$, $Xk^{-/-}$, and double-knockout $Kel^{-/-}Xk^{-/-}$ mice have been produced.[13,16] In studies with erythrocytes from these sets of knockout mice, Kell and XK proteins were recently shown to be functionally coupled with divalent cation transport systems.[13,16] In the present study, we investigated the pathological features of the neuromuscular system in $Kel^{-/-}$, $Xk^{-/-}$, and $Kel^{-/-}Xk^{-/-}$ mice, to elucidate the underlying pathophysiology of neuromuscular symptoms in MLS patients.

Materials and Methods

Mice

Targeted gene disruption was used to establish female $Kel^{-/-}$ 129/SvJ mice and male $Xk^{-/y}$ 129/SvJ mice. The targeting constructs, gene targeting methods, and characterization of the $Kel^{-/-}$ and $Xk^{-/y}$ mice were as described previously by Zhu et al[13] and Rivera et al.[16] To produce knockout mouse lines on a C57BL/6 congenic background, female $Kel^{-/-}$ and male $Xk^{-/y}$ mice were mated to C57BL/6 mice, purchased from Charles River Laboratories International (Wilmington, MA), and backcrossed for 10 generations. Wild-type (WT) mice were obtained by breeding N10 heterozygous or hemizygous offspring. N10 male $Kel^{-/-}$ and female $Xk^{-/-}$ mice were mated to produce N11 female $Kel^{+/-}$ $Xk^{+/-}$ and male $Kel^{+/-}Xk^{-/y}$ mice. These mice were mated to produce a double-knockout $Kel^{-/-}Xk^{-/-}$ mouse line. All mice used in this study were on a C57BL/6 congenic background. All animals were housed and handled according to protocols approved by the institutional animal care and use committee at the New York Blood Center. At least three mice from each of four different age groups were used for histopathological studies from three different experimental genotypes (knockout mouse lines) and WT mice. The age groups studied ranged from 6 to 18 months. $Xk^{-/-}$ mice ($n = 7$) and matching WT mice ($n = 8$), aged 10 to 18 months, were housed individually for 5 to 7 months in cages with exercise wheels connected to a digital magnetic counter activated by wheel rotation.

Pathology

All mice were weighed. After deep anesthesia using isoflurane (USP) (Baxter Healthcare, Deerfield, IL), mice were transcardially perfused with PBS for 10 minutes, which was followed by 4% paraformaldehyde perfusion. Brain, spinal cord with attached spinal roots, and bilateral sciatic nerves were removed. Parts of the sciatic nerves and lumbar spinal cord were fixed in 3% glutaraldehyde in 0.1 mol/L sodium cacodylate buffer (pH 7.3) for electron microscopy. The remainder of the sciatic nerve and spinal cord tissue was further fixed in 4% paraformaldehyde for paraffin embedding. During PBS perfusion, the gastrocnemius, quadriceps femoris, and triceps brachii muscles were isolated, snap-frozen in isopentane prechilled with liquid nitrogen, and stored at −80°C.

After paraffin embedding, cross sections (8 μm) were cut from the cervical enlargement, midthoracic segment, and lumbar enlargement and were stained with H&E. Sciatic nerves were sectioned (5 μm thick) and stained with H&E. Cryosections (5 μm thick) of gastrocnemius, quadriceps femoris, and triceps brachii muscles were stained with H&E and modified Gömöri trichrome stain. Skeletal muscles were stained with NADH–tetrazolium reductase, ATPases (pH 4.6 and pH 9.4), nonspecific esterase, and acid phosphatase, according to standard methods.

Sections (1 μm thick) were cut from eponate-embedded tissue and stained with Toluidine Blue and counterstained with safranin. Cross sections of the ventral quarter of spinal cord and both cross sections and longitudinal sections of anterior roots were obtained from 28 mice, including 21 knockout mice (Table 1). Sciatic nerves were obtained from 38 mice, including 25 knockout mice (Table 2). From these, 7 knockout and 4 WT mice were selected for further study by electron microscopy. Ultrathin sections (80 nm thick) were stained with uranyl acetate and lead citrate for examination using an EM-410 transmission electron microscope (Philips, Amsterdam, The Netherlands).

Table 1 Frequency of Giant Axons and/or Paranodal Demyelination in the Anterior Column of the Spinal Cord and Ventral Roots

Genotype	Age (months)	Cases (no.)	Score*			
			−	+	++	+++
Nonexercised mice						
WT	17	6	4	2	0	0
$Xk^{-/-}$	17	4	1	0	1	2
$Kel^{-/-}$	12	5	1	1	0	3
$Kel^{-/-}$	17	3	0	0	0	0
$Kel^{-/-}Xk^{-/-}$	17	6	0	0	0	6
Exercised mice						
WT	18	1	0	1	0	0
$Xk^{-/-}$	18	3	0	0	0	3

*Scoring is based on 10 randomly selected high-power fields. −, absence of giant axons; +, 1 giant axons and/or paranodal demyelination; ++, 2 to 3 giant axons and/or paranodal demyelinations; +++, ≥4 giant axons and/or paranodal demyelinations.

Table 2 Frequency of Giant Axons and/or Paranodal Demyelination in the Sciatic Nerve

Genotype and condition	Older mice					Younger mice				
		Score*					Score*			
	Cases (no.)	−	+	++	+++	Cases (no.)	−	+	++	+++
Nonexercised	17 months					6–12 months				
WT	7	6	1	0	0	4	4	0	0	0
Xk$^{-/-}$	4	2	2	0	0	3	3	0	0	0
Kel$^{-/-}$	2	1	0	1	0	3	3	0	0	0
Kel$^{-/-}$*Xk*$^{-/-}$	5	2	2	1	0	4	4	0	0	0
Exercised	16–19 months					10 months				
WT	1	1	0	0	0	1	1	0	0	0
Xk$^{-/-}$	2	1	0	1	0	2	1	1	0	0

*Scoring as defined for Table 1, except based on one cross section of sciatic nerve.

Results

Spinal Cord, Ventral Roots, and Sciatic Nerves

The most striking change seen on 1-μm-thick sections stained with Toluidine Blue was the presence of giant axons in the sciatic nerve and in the anterior column of the spinal cord (Figures 1 and 2). The giant axons were of various sizes and contained mostly pale, homogeneous axoplasm. Occasionally, they contained irregularly distributed osmium-dense particles (Figures 1E and 2E). The myelin sheaths of most giant axons were thinner than expected from their diameter on cross sections (Figures 1C and 2B). On longitudinal sections, the thickness of myelin sheaths was frequently irregular over the length of an internode and exhibited paranodal demyelination, with an extended gap in the myelin sheath between internodes (Figures 1D and 2D and 2F). In addition to the giant axons, a few small nerve fibers were surrounded by thicker myelin sheaths than expected from their diameters (Figure 1F).

Ultrastructurally, most giant axons had thinner myelin sheaths than expected from their diameters (Figure 3, A and B) and were filled with irregularly bundled neurofilaments (NFs) (Figure 3C). Microtubules and other organelles were sparsely dispersed among the bundles of NFs (Figure 3, D–F). Other findings included clustering of microtubules, dense lamellar bodies, and membranous vesicles, as well as membranous structures involving the adaxon of Schwann cells, which may indicate adaxonal degeneration of Schwann cells (Figure 3, G and H). As in the 1-μm-thick sections examined under light microscopy, occasional small axons had thicker myelin sheaths than expected (Figure 3I).

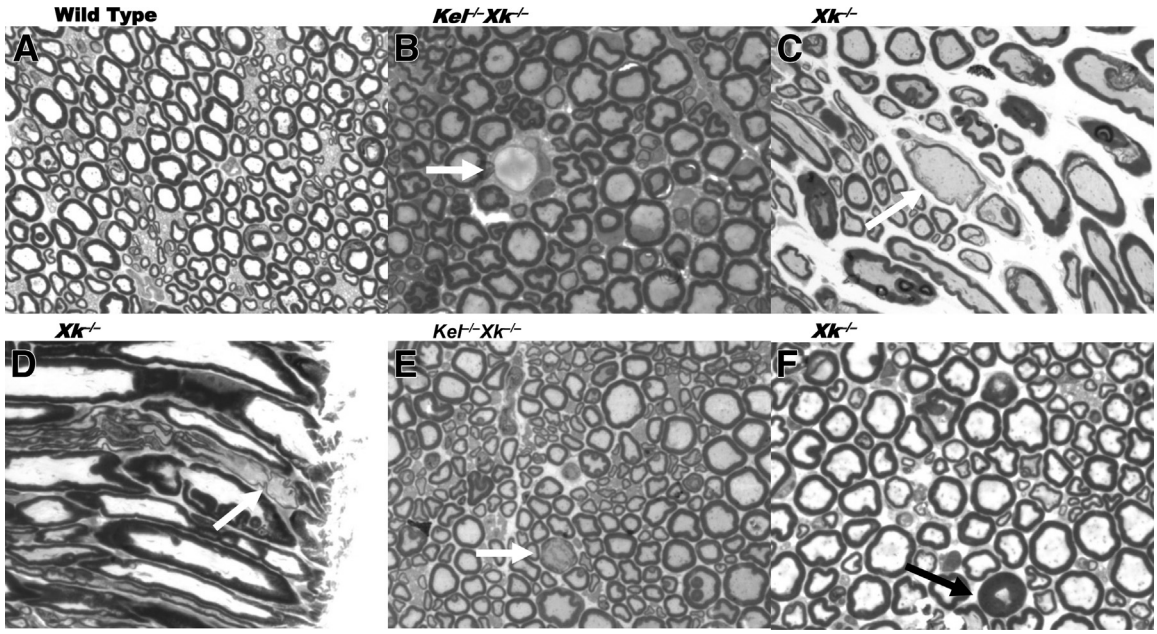

Figure 1 Giant axons (**arrows**) in mouse sciatic nerve. **A:** Transverse section (WT). **B:** Large demyelinated axon from transverse section (*Kel*$^{-/-}$*Xk*$^{-/-}$). **C:** Large axons with thin myelin sheath from longitudinal section (*Xk*$^{-/-}$). **D:** A portion of an internode with partial demyelination from a longitudinal section (*Xk*$^{-/-}$). **E:** Large axon with disrupted myelin sheath and unevenly distributed osmium-dense material (*Kel*$^{-/-}$*Xk*$^{-/-}$). **F:** Atrophic axon with thick myelin sheath (*Xk*$^{-/-}$). Sections are 1 μm thick. Toluidine Blue stain. Original magnification, ×1000.

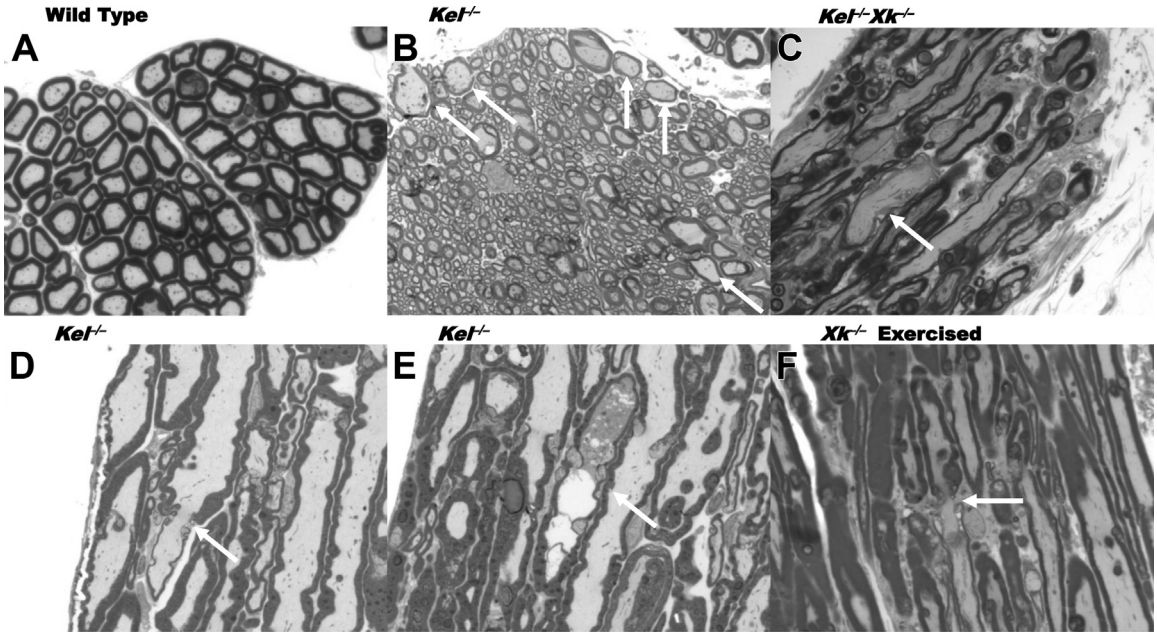

Figure 2 Giant axons (**arrows**) in the anterior column and ventral root of mouse spinal cord. **A:** Transverse section of the anterior column (from WT mice). **B:** Several large axons with relatively thin myelin sheaths on a transverse section of anterior column ($Kel^{-/-}$). **C** and **D:** Irregular thickness of myelin sheath with paranodal demyelination and partial detachment of myelin leaflets in a longitudinal section of the ventral root [$Kel^{-/-}Xk^{-/-}$ (**C**) and $Kel^{-/-}$ (**D**)]. **E:** Enlarged axon packed with osmium-dense particles and vacuoles with partial disruption of myelin sheath from a longitudinal section of the ventral root ($Kel^{-/-}$). **F:** Paranodal demyelination from a longitudinal section of the ventral root of exercised mice ($Xk^{-/-}$). Sections are 1 μm thick. Toluidine Blue stain. Original magnification, ×1000.

The density of giant axons was clearly higher in the anterior column of the spinal cord, especially in the subpial zone, relative to that of the sciatic nerve.

All three genotypes had giant axons of similar appearance, but giant axons were more frequent in $Kel^{-/-}Xk^{-/-}$ mice than in $Kel^{-/-}$ or $Xk^{-/-}$ (Tables 1 and 2). Although the number of mice in each group was small, there was an appreciable tendency toward more giant axons in older mice, and in exercised mice (Tables 1 and 2). WT mice also had occasional large axons, but these were of smaller diameter than in experimental animals, and all had myelin sheaths of normal thickness (ie, as expected from their diameters) (Figure 2A).

Skeletal Muscle

In young $Xk^{-/-}$, $Kel^{-/-}$, and $Xk^{-/-}Kel^{-/-}$ mice, it was hard to discern any obvious pathology. Skeletal muscles in older $Xk^{-/-}$ and $Xk^{-/-}Kel^{-/-}$ mice were clearly abnormal, with variation in muscle fiber sizes, frequent internalized nuclei (Figure 4D), occasional muscle fiber splitting, and atrophic fibers (Figure 4, B–D). Atrophic fibers were mostly angulated and singly scattered among other fibers (Figure 4, B–D). Occasional angulated atrophic fibers found in all experimental genotypes had diffusely basophilic sarcoplasm with a faintly fluffy quality to it (Figure 4C). There was no necrosis in any genotype, but regenerating fibers were occasionally noted in exercised $Xk^{-/-}$ mice (Supplemental Tables S1 and S2). No endomysial fibrosis was noted, and there was no fiber-type atrophy. Angulated fibers (Supplemental Table S1) and internalized nuclei (Supplemental Table S2) were frequently present in $Xk^{-/-}$ mice (to a greater extent in $Xk^{-/-}Kel^{-/-}$ mice, and most frequently in exercised $Xk^{-/-}$ mice). The findings in $Kel^{-/-}$ mice did not differ significantly different from those in WT.

Discussion

Greater numbers of giant axons with varying degrees of paranodal demyelination were observed in the anterior column of the spinal cord and ventral roots of spinal nerve in all three lines of knockout mice, compared with WT mice. Giant axons typically result from disturbances in function or structure of NFs, which are a major component of vertebrate neural cytoskeleton and are associated with axonal transport. Disruption of NF architecture at many levels can result in giant axon formation due to NF accumulation. Giant axonopathy, which has been described in many unrelated conditions, is the apparent end result of various toxic and metabolic derangements.[17–20] The histopathological features observed in the present study are similar to drug-induced nerve damage caused by iminodipropionitrile,[21] doxorubicin (Adriamycin),[22] quelamycin,[23] or vincristine,[24] in which axoplasmic disturbance induced accumulation of NF, leading to formation of giant axons. NF accumulation is also found in amyotrophic lateral sclerosis.[25,26]

In $Xk^{-/-}$ and $Kel^{-/-}$ mice, giant axonal changes were more prominent in the spinal cord than in sciatic nerve, suggesting anterograde progression of the pathological features. In iminodipropionitrile-induced damage, giant axons with NF accumulation are caused by the disruption of

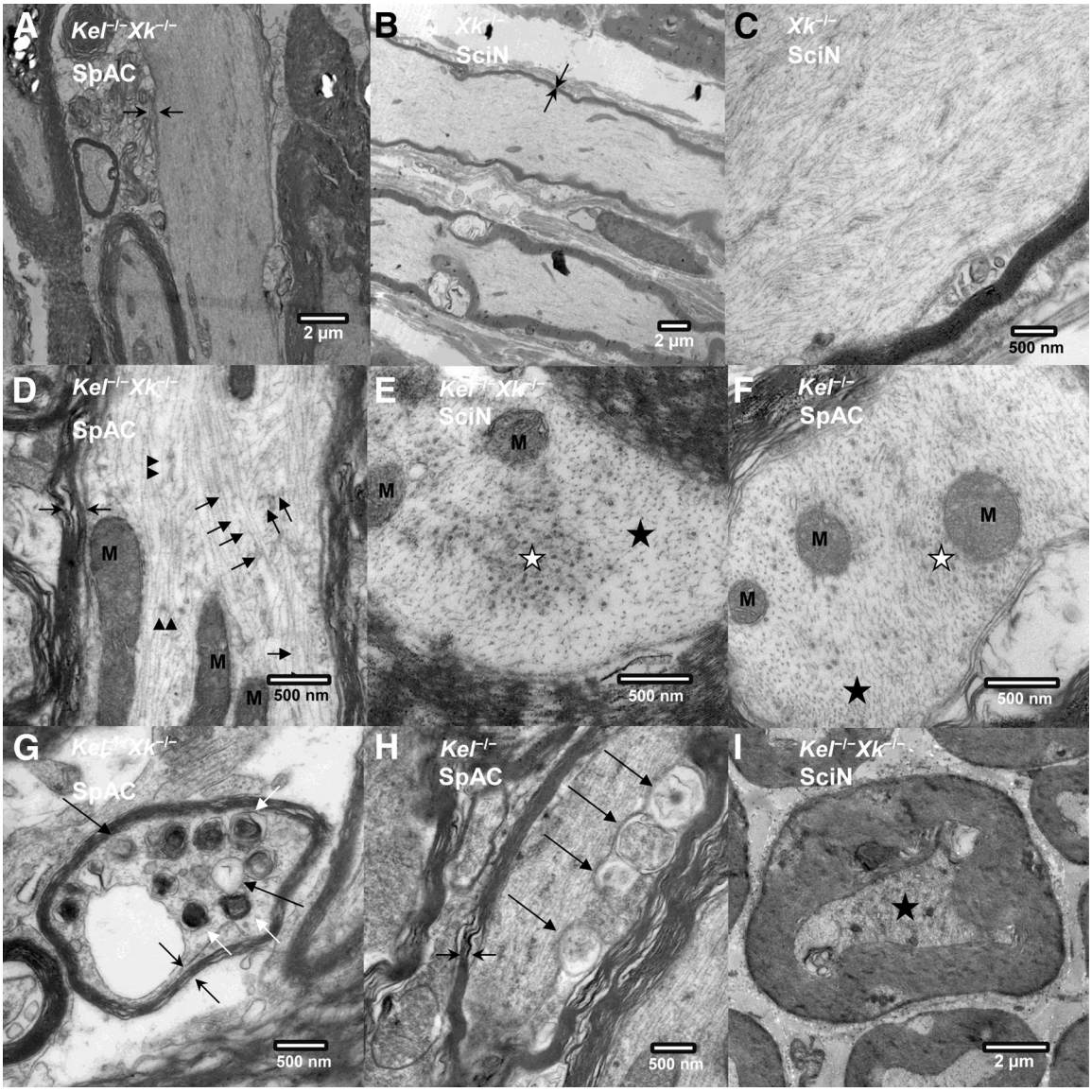

Figure 3 Ultrastructural details of giant axons in spinal cord and sciatic nerve. **A:** Giant axon with an extremely attenuated myelin sheath in the anterior column of the spinal cord ($Kel^{-/-}Xk^{-/-}$). **B:** Giant axon with an extremely attenuated myelin sheath in the sciatic nerve ($Xk^{-/-}$). **C:** Giant axon with irregular accumulation of NFs and apparent absence of other organelles in the sciatic nerve ($Xk^{-/-}$). **D:** Giant axon with a thin myelin sheath containing irregularly arranged NFs and sparsely scattered microtubules in the anterior column of the spinal cord ($Kel^{-/-}Xk^{-/-}$). **E:** Segregation of microtubules from NFs on a cross section of the sciatic nerve ($Kel^{-/-}Xk^{-/-}$). **F:** Irregularly dispersed microtubules in the anterior column of the spinal cord ($Kel^{-/-}$). **G:** Accumulation of dense lamellar bodies and membranous vesicles indicating axonal degeneration in the anterior column of the spinal cord ($Kel^{-/-}Xk^{-/-}$). **H:** Membranous structures involving the adaxon of a Schwann cell in the anterior column of the spinal cord ($Kel^{-/-}$). **I:** Atrophic axon with contracted axon surrounded by a thick myelin sheath containing osmium-dense particles in the sciatic nerve of $Kel^{-/-}Xk^{-/-}$ mice. Symbols: **opposing arrows**, thin or absent MS; **short black arrow** or **black star**, NF; **long black arrow**, MV; **black arrowhead** or **white star**, MT; **white arrow**, DLB. Sections are 80 nm thick. Scale bars: 2 μm (**A**, **B**, and **I**); 500 nm (**C**—**H**). DLB, dense lamellar body; M, mitochondria; MS, myelin sheath; MT, microtubule; MV, membranous vesicles; SciN, sciatic nerve; SpAC, anterior column of the spinal cord.

side-arms connecting NFs and microtubules.[21] Furthermore, NFs are closely associated with αII/βII-spectrin (non-erythroid spectrin, or fodrin) *in vivo*[5–7] and βIIΣ1-spectrin interacts with NF light-chain (NF-L) proteins *in vitro*, and similarly with actin.[27] αII Spectrin is involved in the paranodal complex that links axo−glial junctions to axonal cytoskeleton.[28] Therefore, XK may interact with the spectrin−actin cytoskeletal complex through binding to 4.1R,[5–7,29] and may associate with the NF-L network in axons and be involved in axonal transport. XK may interact directly or indirectly with NFs, particularly with NF-L. Absence of XK may be one of the mechanisms for disturbance of the slow component of axonal transport, NF accumulation, and the resultant giant axon formation in $Xk^{-/-}$ mice. These neuropathological findings correlate with the findings of motor abnormalities indicative of peripheral neuromuscular dysfunction for $Kel^{-/-}$ mice.[13]

Disruption of ion homeostasis due to dysfunction of the 4.1R protein subcomplex in the absence of XK may be one of the causes of paranodal demyelination and may also

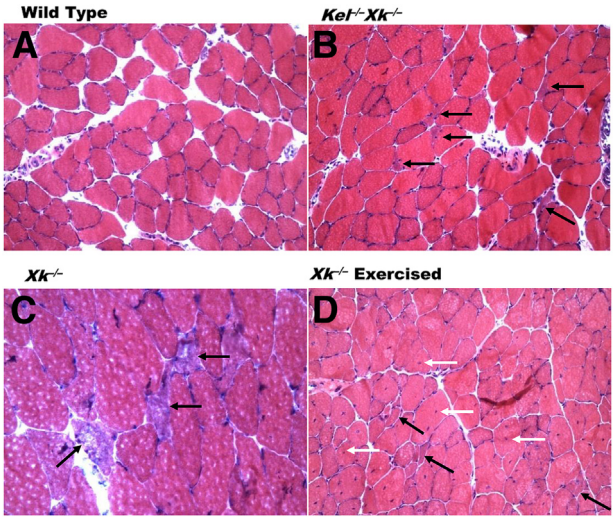

Figure 4 Skeletal muscle abnormalities. **A:** WT quadriceps femoris. **B** and **C:** Triceps brachii with angulated fibers (**black arrows**) of $Kel^{-/-}Xk^{-/-}$ (**B**) and $Xk^{-/-}$ (**C**) mice. **D:** Quadriceps femoris of $Xk^{-/-}$ exercised mice with angulated fibers (**black arrows**) and internalized nuclei (**white arrow**). H&E stain. Sections are 5 μm thick. Original magnification: ×200 (**A**, **B**, and **D**); ×400 (**C**).

affect axonal transport, leading further to giant axon formation. The XK-binding FERM domain of 4.1 proteins is a recruiter of many functional proteins, including ion transporters and proteins involved in signal transduction, forming a cytoskeleton−membrane regulatory macrocomplex.[30] *Ex vivo* studies of the physiological function of XK−Kell complex using $Xk^{-/-}$, $Kel^{-/-}$, and $Kel^{-/-}Xk^{-/-}$ mice have shown that XK and Kell are associated with cation transport systems involved in ion homeostasis and that Kell may control XK, either directly or indirectly.[16]

Although giant axons have not been reported in patients with MLS, the nonspecific findings found on sural nerve biopsy of minimal axonal neuropathy with fibrosis and evidence of active degeneration[4,31,32] are consistent with changes in the distal portion of a nerve in which there is proximal giant axonopathy. Axonal degeneration is an expected consequence of failure of orderly axoplasmic flow.[33] If a similar pathological process occurs in MLS patients, negative electrodiagnostic findings would be expected early in the course of MLS, unless the study includes the proximal loop of the circuit (H reflex, but this is not routinely performed). Although elevated creatine kinase, usually interpreted as an indication of muscle damage (primary myopathy), is typically observed during the asymptomatic phase in MLS patients,[34] muscle weakness may be the result of conduction blockage due to paranodal demyelination, rather than to primary myopathy. This may also explain the lack of pathological changes in muscle biopsy early in the disease course, whereas biopsies from patients with longer-term disease show evidence of neurogenic atrophy.[4]

Muscle abnormalities were readily recognizable in $Xk^{-/-}$ mice, still more evident in $Kel^{-/-}Xk^{-/-}$ mice, and most abundant in exercised $Xk^{-/-}$ mice. In contrast, there was no obvious pathology in the muscles of $Kel^{-/-}$ mice. Kell and XK proteins in human skeletal muscle differ in both amount[12,14] and distribution.[15] XK is abundant and present in sarcoplasmic membranes confined to the sarcoplasmic reticulum, as indicated by a distinctive honeycomb-like pattern of anti-XK immunoreactivity in type 2 fibers. These type 2 fibers are atrophic in MLS.[15] Kell is present at much lower levels than XK, and is present in sarcolemma. The excess XK could exist either as a monomer or coupled with a protein other than Kell. Because multiple isoforms of 4.1R are known to be present in skeletal muscles,[35] it is plausible that XK binds to 4.1R or to other 4.1 proteins as part of a large protein complex. In brain, the 4.1R isoform and 4.1G bind with a fodrin−F-actin complex.[36]

In human MLS, mixed neuropathic and myopathic abnormalities are observed.[1,4] Although the giant axons that we observed indicated neuropathy, the muscle findings seen in $Xk^{-/-}$ and $Kel^{-/-}Xk^{-/-}$ mice (eg, weak nonspecific esterase staining and absence of fiber-type grouping) were more consistent with myopathy.

The muscle weakness and atrophy of MLS patients increases with advancing disease,[1,4] which is consistent with our findings in younger versus older mice. In humans, the disease affects mainly the lower limbs and is more pronounced distally[1,4] (as is typical of neuropathic diseases in which the longest axons are most vulnerable), which differs from our present findings of more proximal involvement. Our data showing giant axon formation with different degrees of paranodal demyelination of sciatic nerve and lumbar spinal cord are consistent with muscle weakness and generalized areflexia indicative of peripheral nervous system involvement.[1,4]

Ultimately, the critical factor in MLS and the role of the Kell−XK complex in pathogenicity remain unknown. Our neuropathology data demonstrate the presence of giant axons in both $Xk^{-/-}$ and $Kel^{-/-}$ mice, which is more marked in $Kel^{-/-}Xk^{-/-}$ mice, suggesting a possible structural and functional association of Kell and XK in neuronal cells, as has been demonstrated in red blood cells.[16] The importance of the Kell−XK complex in neuronal cells can be predicted based on the evolutionary patterns of the Kell system involving signaling pathways through Kell (with endothelin-3-converting enzyme activity)−endothelin-3 (ET-3)−endothelin receptor B. Kell appeared in warm-blooded vertebrates later[37] than did XK,[38,39] and linked to the pre-existing vertebrate gene product XK apparently to modify its function. This signaling path is the most recent addition to the pre-existing endothelin systems and may control the role of the functional protein subunit at the 4.1R−spectrin−actin ternary complex, either by a direct effect on XK or indirectly through proteins in the 4.1R functional protein subunit.[16] If this ET-3 signaling path is the object of Kell in the Kell−XK complex, then a reduced level of Kell in absence of XK will have a critical role in MLS. Critical evaluation of this protein subunit as a one functional unit may be required. The dearth of information regarding tissue and cellular expression of

Kell and XK has hampered studies of the pathophysiology of MLS. Critical evaluations of XK and Kell and the proteins associated with these two proteins, such as in the 4.1R subunit of functional protein complex in the cytoskeleton, may provide valuable insights.

Humans without Kell (Kell-null red blood cell phenotype) appear to be clinically normal, although no neuromuscular pathological studies of such subjects have yet been reported. This species difference may be due to differences between human and mouse Kell, although the proteins have functional and structural similarities (74% amino acid sequence identity), in addition to the inherent biophysiological differences between human and mouse. For example, both mouse and human Kell proteins have substrate preference for big ET-3, but the preference of human Kell for big ET-3 appears to be stronger than that of mouse Kell, and mouse Kell has a greater ability to cleave big ET-1 and big ET-2 showing higher redundancy.[40,41]

In conclusion, $Kel^{-/-}$, $Xk^{-/-}$, and $Kel^{-/-}Xk^{-/-}$ mice exhibit pathological changes that could explain some of the neuromuscular symptoms in MLS patients. These knockout mouse models could be informative for further investigations into the underlying mechanisms of the pathological features of MLS, and also in chorea–acanthocytosis, which is a genetically distinct but phenotypically similar neuroacanthocytosis syndrome that similarly manifests with acanthocytosis and basal ganglia degeneration.[42,43]

Acknowledgments

We thank Dr. Roy Rhodes (UMDNJ-Robert Wood Johnson Medical School, Newark and Piscataway, NJ) for consultation on electron micrographs, Dr. Yanfeng Zhong (Peking University Health Science Center, China) for consultation on pathology laboratory procedures, and staff of the former Membrane Biochemistry Laboratory of the New York Blood Center for technical support and breeding mouse colonies.

Supplemental Data

Supplemental material for this article can be found at *http://dx.doi.org/10.1016/j.ajpath.2013.11.013*.

References

1. Danek A, Rubio JP, Rampoldi L, Ho M, Dobson-Stone C, Tison F, Symmans WA, Oechsner M, Kalckreuth W, Watt JM, Corbett AJ, Hamdalla HH, Marshall AG, Sutton I, Dotti MT, Malandrini A, Walker RH, Daniels G, Monaco AP: McLeod neuroacanthocytosis: genotype and phenotype. Ann Neurol 2001, 50:755–764
2. Danek A, Walker RH: Neuroacanthocytosis. Curr Opin Neurol 2005, 18:386–392
3. Jung HH, Danek A, Frey BM: McLeod syndrome: a neurohaematological disorder. Vox Sang 2007, 93:112–121
4. Hewer E, Danek A, Schoser BG, Miranda M, Reichard R, Castiglioni C, Oechsner M, Goebel HH, Heppner FL, Jung HH: McLeod myopathy revisited: more neurogenic and less benign. Brain 2007, 130:3285–3296
5. Ohno N, Terada N, Yamakawa H, Komada M, Ohara O, Trapp BD, Ohno S: Expression of protein 4.1G in Schwann cells of the peripheral nervous system. J Neurosci Res 2006, 84:568–577
6. Salomao M, Zhang X, Yang Y, Lee S, Hartwig JH, Chasis JA, Mohandas N, An X: Protein 4.1R-dependent multiprotein complex: new insights into the structural organization of the red blood cell membrane. Proc Natl Acad Sci USA 2008, 105:8026–8031
7. Scott C, Phillips GW, Baines AJ: Properties of the C-terminal domain of 4.1 proteins. Eur J Biochem 2001, 268:3709–3717
8. Baines AJ: Evolution of the spectrin-based membrane skeleton. Transfus Clin Biol 2010, 17:95–103
9. Clapéron A, Hattab C, Armand V, Trottier S, Bertrand O, Ouimet T: The Kell and XK proteins of the Kell blood group are not co-expressed in the central nervous system. Brain Res 2007, 1147:12–24
10. Daniels GL, Weinauer F, Stone C, Ho M, Green CA, Jahn-Jochem H, Offner R, Monaco AP: A combination of the effects of rare genotypes at the XK and KEL blood group loci results in absence of Kell system antigens from the red blood cells. Blood 1996, 88:4045–4050
11. Lee S, Sha Q, Wu X, Calenda G, Peng J: Expression profiles of mouse Kell, XK, and XPLAC mRNA. J Histochem Cytochem 2007, 55:365–374
12. Ho M, Chelly J, Carter N, Danek A, Crocker P, Monaco AP: Isolation of the gene for McLeod syndrome that encodes a novel membrane transport protein. Cell 1994, 77:869–880
13. Zhu X, Rivera A, Golub MS, Peng J, Sha Q, Wu X, Song X, Kumarathasan P, Ho M, Redman CM, Lee S: Changes in red cell ion transport, reduced intratumoral neovascularization, and some mild motor function abnormalities accompany targeted disruption of the mouse Kell gene (Kel). Am J Hematol 2009, 84:492–498
14. Russo D, Wu X, Redman CM, Lee S: Expression of Kell blood group protein in nonerythroid tissues. Blood 2000, 96:340–346
15. Jung HH, Russo D, Redman C, Brandner S: Kell and XK immunohistochemistry in McLeod myopathy. Muscle Nerve 2001, 24:1346–1351
16. Rivera A, Kam SY, Ho M, Romero JR, Lee S: Ablation of the Kell/Xk complex alters erythrocyte divalent cation homeostasis. Blood Cells Mol Dis 2013, 50:80–85
17. Anthony DC, Giangaspero F, Graham DG: The spatio-temporal pattern of the axonopathy associated with the neurotoxicity of 3,4-dimethyl-2,5-hexanedione in the rat. J Neuropathol Exp Neurol 1983, 42:548–560
18. Fabrizi GM, Cavallaro T, Angiari C, Bertolasi L, Cabrini I, Ferrarini M, Rizzuto N: Giant axon and neurofilament accumulation in Charcot-Marie-Tooth disease type 2E. Neurology 2004, 62:1429–1431
19. Monaco S, Autilio-Gambetti L, Zabel D, Gambetti P: Giant axonal neuropathy: acceleration of neurofilament transport in optic axons. Proc Natl Acad Sci USA 1985, 82:920–924
20. Vogel P, Gabriel M, Goebel HH, Dyck PJ: Hereditary motor sensory neuropathy type II with neurofilament accumulation: new finding or new disorder? Ann Neurol 1985, 17:455–461
21. Griffin JW, Fahnestock KE, Price DL, Hoffman PN: Microtubule-neurofilament segregation produced by beta, beta′-iminodipropionitrile: evidence for the association of fast axonal transport with microtubules. J Neurosci 1983, 3:557–566
22. Cho ES: Toxic effects of Adriamycin on the ganglia of the peripherial nervous system: a neuropathological study. J Neuropathol Exp Neurol 1977, 36:907–915
23. Jortner BS, Cho ES: Neurotoxicity of quelamycin in the rat. Neurotoxicology 1981, 2:789–792
24. Cho ES, Lowndes HE, Goldstein BD: Neurotoxicology of vincristine in the cat. Morphological study. Arch Toxicol 1983, 52:83–90
25. Chou SM, Wang HS, Komai K: Colocalization of NOS and SOD1 in neurofilament accumulation within motor neurons of amyotrophic lateral sclerosis: an immunohistochemical study. J Chem Neuroanat 1996, 10:249–258
26. Gold BG: The pathophysiology of proximal neurofilamentous giant axonal swellings: implications for the pathogenesis of amyotrophic lateral sclerosis. Toxicology 1987, 46:125–139

27. Macioce P, Gandolfi N, Leung CL, Chin SS, Malchiodi-Albedi F, Ceccarini M, Petrucci TC, Liem RK: Characterization of NF-L and betaIISigma1-spectrin interaction in live cells. Exp Cell Res 1999, 250: 142−154
28. Garcia-Fresco GP, Sousa AD, Pillai AM, Moy SS, Crawley JN, Tessarollo L, Dupree JL, Bhat MA: Disruption of axo-glial junctions causes cytoskeletal disorganization and degeneration of Purkinje neuron axons. Proc Natl Acad Sci USA 2006, 103:5137−5142
29. Scott C, Keating L, Bellamy M, Baines AJ: Protein 4.1 in forebrain postsynaptic density preparations: enrichment of 4.1 gene products and detection of 4.1R binding proteins. Eur J Biochem 2001, 268:1084−1094
30. Einheber S, Meng X, Rubin M, Lam I, Mohandas N, An X, Shrager P, Kissil J, Maurel P, Salzer JL: The 4.1B cytoskeletal protein regulates the domain organization and sheath thickness of myelinated axons. Glia 2013, 61:240−253
31. Dotti MT, Battisti C, Malandrini A, Federico A, Rubio JP, Circiarello G, Monaco AP: McLeod syndrome and neuroacanthocytosis with a novel mutation in the XK gene. Mov Disord 2000, 15:1282−1284
32. Dotti MT, Malandrini A, Federico A: Neuromuscular findings in eight Italian families with neuroacanthocytosis. Edited by Danek. A. Neuroacanthocytosis syndromes. Dordrecht, The Netherlands, Springer, 2004, pp 127−138
33. Griffin JW, Price DL, Engel WK, Drachman DB: The pathogenesis of reactive axonal swellings: role of axonal transport. J Neuropathol Exp Neurol 1977, 36:214−227
34. Walker RH, Danek A, Uttner I, Offner R, Reid M, Lee S: McLeod phenotype without the McLeod syndrome. Transfusion 2007, 47:299−305
35. Kontrogianni-Konstantopoulos A, Huang SC, Benz EJ Jr.: A non-erythroid isoform of protein 4.1R interacts with components of the contractile apparatus in skeletal myofibers. Mol Biol Cell 2000, 11: 3805−3817
36. Kontrogianni-Konstantopoulos A, Frye CS, Benz EJ Jr., Huang SC: The prototypical 4.1R-10-kDa domain and the 4.1G-10-kDa paralog mediate fodrin-actin complex formation. J Biol Chem 2001, 276: 20679−20687
37. Bland ND, Pinney JW, Thomas JE, Turner AJ, Isaac RE: Bioinformatic analysis of the neprilysin (M13) family of peptidases reveals complex evolutionary and functional relationships. BMC Evol Biol 2008, 8:16
38. Calenda G, Peng J, Redman CM, Sha Q, Wu X, Lee S: Identification of two new members, XPLAC and XTES, of the XK family. Gene 2006, 370:6−16
39. Peng J, Redman CM, Wu X, Song X, Walker RH, Westhoff CM, Lee S: Insights into extensive deletions around the XK locus associated with McLeod phenotype and characterization of two novel cases. Gene 2007, 392:142−150
40. Lee S, Russo DC, Pu J, Ho M, Redman CM: The mouse Kell blood group gene (Kel): cDNA sequence, genomic organization, expression, and enzymatic function. Immunogenetics 2000, 52:53−62
41. Lee S, Lin M, Mele A, Cao Y, Farmar J, Russo D, Redman C: Proteolytic processing of big endothelin-3 by the Kell blood group protein. Blood 1999, 94:1440−1450
42. Jung HH, Danek A, Walker RH, Frey BM, Gassner C: McLeod Neuroacanthocytosis Syndrome. In GeneReviews [Internet]. University of Washington, Seattle; 1993−2013. Available at http://www.ncbi.nlm.nih.gov/books/NBK1354, last revised May 17, 2012
43. Jung HH, Danek A, Walker RH: Neuroacanthocytosis syndromes. Orphanet J Rare Dis 2011, 6:68